Zika virus leads to olfactory disorders in mice by targeting olfactory ensheathing cells

Jia Zhou,[a,g] Meng-Yue Guan,[b,g] Rui-Ting Li,[a,g] Yi-Ni Qi,[c,g] Guan Yang,[c] Yong-Qiang Deng,[a] Xiao-Feng Li,[a] Liang Li,[d] Xiao Yang,[c] Jian-Feng Liu,[e] and Cheng-Feng Qin[a,f,*]

[a]State Key Laboratory of Pathogen and Biosecurity, Beijing Institute of Microbiology and Epidemiology, Beijing 100071, China
[b]Department of Respiratory Medicine, Beijing Hospital of Traditional Chinese Medicine, Capital Medical University, Beijing 10010, China
[c]State Key Laboratory of Proteomics, National Center for Protein Science (Beijing), Beijing Institute of Lifeomics, Beijing 102206, China
[d]Shenzhen Institutes of Advanced Technology, Chinese Academy of Sciences, Shenzhen 518055, China
[e]Department of Otorhinolaryngology, China-Japan Friendship Hospital, Beijing 100029, China
[f]Research Unit of Discovery and Tracing of Natural Focus Diseases, Chinese Academy of Medical Sciences, Beijing, China

eBioMedicine
2023;89: 104457
Published Online xxx
https://doi.org/10.1016/j.ebiom.2023.104457

Summary

Background Zika virus (ZIKV) is an emerging arbovirus of the genus flavivirus that is associated with congenital Zika syndrome (CZS) in newborns. A wide range of clinical symptoms including intellectual disability, speech delay, coordination or movement problems, and hearing and vision loss, have been well documented in children with CZS. However, whether ZIKV can invade the olfactory system and lead to post-viral olfactory dysfunction (PVOD) remains unknown.

Methods We investigated the susceptibility and biological responses of the olfactory system to ZIKV infection using mouse models and human olfactory organoids derived from patient olfactory mucosa.

Findings We demonstrate that neonatal mice infected with ZIKV suffer from transient olfactory dysfunction when they reach to puberty. Moreover, ZIKV mainly targets olfactory ensheathing cells (OECs) and exhibits broad cellular tropism colocalizing with small populations of mature/immature olfactory sensory neurons (mOSNs/iOSNs), sustentacular cells and horizontal basal cells in the olfactory mucosa (OM) of immunodeficient AG6 mice. ZIKV infection induces strong antiviral immune responses in both the olfactory mucosa and olfactory bulb tissues, resulting in the upregulation of proinflammatory cytokines/chemokines and genes related to the antiviral response. Histopathology and transcriptomic analysis showed typical tissue damage in the olfactory system. Finally, by using an air-liquid culture system, we showed that ZIKV mainly targets sustentacular cells and OECs and support robust ZIKV replication.

Interpretation Our results demonstrate that olfactory system represents as significant target for ZIKV infection, and that PVOD may be neglected in CZS patients.

Funding Stated in the acknowledgment.

Keywords: Zika virus; Olfactory pathway; Olfactory dysfunction; Immune response

Introduction

Zika virus (ZIKV) is a member of the *Flaviviridae* family that was first isolated from a sentinel rhesus monkey in Uganda in 1947[1] and is primarily transmitted to humans via the bite of infected Aedes mosquitoes. Person-to-person transmission can also occur via sexual contact, mother to child vertical transmission, blood transfusion and organ transplantation. Although the first case of human ZIKV infection was detected in the early 1950s, only a few sporadic human cases of ZIKV infection were reported in the next few decades.[2] However, ZIKV rapidly swept through dozens of countries and territories around the world since its first epidemic in 2007 in West Pacific Micronesia.[3–6] To date, ZIKV has adapted to achieve persistent endemic circulation and widespread transmission,[7,8] and it represents a global

*Corresponding author.
E-mail address: qincf@bmi.ac.cn (C.-F. Qin).
[g]These authors contributed equally: Jia Zhou, Meng-Yue Guan, Rui-Ting Li, Yi-Ni Qi.

Research in context

Evidence before this study

Zika virus (ZIKV) represents a global epidemic risk and public health threat due to its widespread transmission and severe neurological complications. The postnatal developmental sequelae of affected children with intrauterine ZIKV infection seem to be severe and are still not fully understood and easy to neglect. Evidence indicates that ZIKV can infect the tissues of olfactory system, which has been hypothesized to be the target of several pathogens including neurotropic flaviviruses. However, whether olfactory disorder is one of the symptoms in the ZIKV affected children and the susceptibility and biological responses of olfactory system to ZIKV infection are largely unknown.

Added value of this study

In this study, we investigated the susceptibility and biological responses of the olfactory system to ZIKV infection using both *in vivo* and *in vitro* models. We first reported transient olfactory disorder as a sequela of ZIKV infection in neonatal mice. We demonstrated robust infection and persistent replication of ZIKV in olfactory system of mice and human olfactory organoids. We further showed that ZIKV mainly targets the olfactory ensheathing cells of olfactory mucosa, and also infects a few of mature and immature olfactory sense neurons, sustentacular cells and horizontal basal cells. Additionally, ZIKV infection induces strong antiviral response and broad-spectrum cytokine secretion in both olfactory mucosa and olfactory bulb tissues, we also note the upregulation of cell death-related genes and downregulation of epithelial cell proliferation according to comprehensive transcriptomic and Luminex assay.

Implications of all the available evidence

Altogether, this study characterized the infectivity and pathogenesis of ZIKV in olfactory system using both *in vitro* and *in vivo* models. Our results provide the first evidence that ZIKV-induced olfactory dysfunction may be one of the neurological sequelae with fetal infection, as well as the experimental foundation for the deepen understanding of ZIKV pathogenesis and discovery of new anti-viral strategies.

epidemic risk and public health threat. Human ZIKV infections were generally asymptomatic or caused only mild self-limited symptoms characterized by lower-grade fever, headache, rash, arthralgia and myalgia in past epidemics.[4,9,10] Notably, the recent outbreak in the Americas has raised substantial global health concerns due to the relationship between ZIKV infection and severe neurological complications,[11–13] including Guillain–Barré syndrome (GBS), acute myelitis and meningoencephalitis in adults and congenital malformations in newborns.[14–16] ZIKV-associated Guillain–Barré syndrome was reported in a limited number of cases during epidemics in French Polynesia, Brazil, Colombia, and other countries,[6] Guillain–Barré syndrome is an autoimmune disease that is characterized by ascending paralysis and polyneuropathy and typically occurs after viral infection.[17] The cause of Guillain–Barré syndrome may be direct ZIKV infection or aberrant autoimmune targeting of the peripheral nervous system.

Congenital infection with ZIKV during pregnancy has been associated with serious neurological malformations known as congenital Zika syndrome (CZS). CZS includes a series of birth defects with unique features, such as severe microcephaly with a partially collapsed skull, thinning of the cerebral cortex with subcortical calcifications, macular scarring and focal pigmentary retinal mottling, congenital contractures, marked early hypertonia and symptoms of extrapyramidal involvement.[18] It seems more detrimental when infections occur during the first trimester of pregnancy, and approximately 10% of affected children have severe CZS.[19] A small proportion of children also suffer from CZS when the pregnant mother is exposed during the second and third trimesters of pregnancy.[20] Children with congenital ZIKV infection at birth always develop complex and long-term medical and developmental outcomes, even children without microcephaly.[20–24] Although studies are sparse, the postnatal developmental sequelae in infants with intrauterine ZIKV infection seem to be severe, including gross motor disabilities, seizures, delayed neurodevelopment, cognitive impairment, vision and hearing loss, ophthalmological abnormalities, hypertonia and spasticity.[18,25] Although most of the affected infants survive, exposure to Zika in utero in the pregnant women also cause fetal loss or neonatal death, which may be associated with several fatal complications such as respiratory distress, dysphagia and epilepsy.[26] To date, the sequalae of infection in children are still not fully understood and easy to miss, especially in those who are asymptomatic at birth.

With advances in research in recent years, increasing evidence has revealed the broad tissue and cell tropism of ZIKV infection in both humans and animals. ZIKV has been detected in the placenta and amniotic fluid of pregnant mothers and the brains and blood of affected fetuses,[27–29] which is consistent with the relationship between ZIKV and microcephaly. As a neurotropic flavivirus, ZIKV was first proven to target human neural progenitor cells (hNPCs) in early research.[30–32] Infection-related cell death and cell cycle dysregulation in hNPCs may be a critical cause of microcephaly and other neurodevelopmental injuries. In addition, neural stem cells, mature neurons, and astrocytes are also permissive to ZIKV infection.[33–35] At the maternal–fetal interface, Hofbauer cells and trophoblasts of placental tissues

were proven to be susceptible to ZIKV infection,[36,37] and ZIKV RNA was also detected in the umbilical cord blood and amniotic fluid.[28,38] Unexpectedly, ZIKV infection can also affect the reproductive system. Female uterine fibroblasts and male spermatogonia and Sertoli cells are target cells of ZIKV infection.[39,40] ZIKV RNA is constantly present in vaginal secretions and sperm for several months after infection,[41–43] and direct infection of reproductive organs in ZIKV may result in testicular injury and infertility.[44,45] In addition, ZIKV can infect several types of human endothelial cells,[46] human skin cells,[47] eye-associated tissues (cornea, optic nerve and neurosensory retina),[48] and spleen and liver tissues,[49] and infectious viral particles are present in several bodily fluids, including saliva, tears and urine in human and animal models; ZIKV infection may result in varying degrees of damage in different types of tissues. Notably, research data show that the human primary respiratory mucosa is susceptible to ZIKV infection.[50] ZIKV RNA was also present in the nasopharyngeal secretions of an infected patient.[51] Recent studies demonstrated that close oronasal contact with an infected person or animal or contaminated bodily fluids increases the risk of acquiring infection,[52] suggesting that the nasal cavity may serve as a target for ZIKV infection.

The nasal mucosa is composed of the respiratory mucosa (RM) and the olfactory mucosa (OM). The primary olfactory system consists of the OM in the peripheral nervous system (PNS) and the central olfactory bulb (OB) and olfactory cortex (OC) in the central nervous system (CNS). The OM lining of the posterodorsal nasal cavity plays a role in the detection of odorants by transmitting olfactory signals to the OB and OC in the CNS via the olfactory nerves. In this pathway, olfactory ensheathing cells (OECs), a specialized type of glia cell, play key roles in the projection of olfactory nerves and supporting axonal regeneration by bounding small nerve fibers together from the OM to OB. In the other hand, the OEC channels of olfactory nerves provide a shortest way for foreign substances to access the CNS. According to previous studies, the olfactory system is susceptible to several viruses,[53–56] including the neurotropic flaviviruses, such as West Nile virus (WNV)[57] and Japanese encephalitis virus (JEV),[58] as well as the newly emerging SARS-CoV-2 causing the current coronavirus disease 2019 (COVID-19) pandemic. Infection of the olfactory system by viruses is a common cause of olfactory disorder, known as post-viral olfactory dysfunction (PVOD). Currently, olfactory dysfunction is considered an early clinical symptom of COVID-19. Evidence indicates that ZIKV can also infect the olfactory cells including cultured human olfactory epithelial cells, mouse olfactory epithelium and olfactory bulb tissues.[59] Additionally, a recent study demonstrated that ZIKV infection was related to long-term olfactory dysfunction in patient with ZIKV-associated GBS.[60] However, the pathogenic properties, distribution and main target cells of ZIKV in the olfactory system, and the changes in olfactory function that occur following ZIKV infection are still largely unknown.

In the present study, we investigated the susceptibility and biological responses of the olfactory system to ZIKV infection using mouse models and human olfactory organoids derived from patient olfactory mucosa. ZIKV replicated well in both olfactory tissues *in vivo* and olfactory organoids ex vivo and mainly targeted OECs. Importantly, transient olfactory dysfunction was observed in immunocompetent adult mice following inoculation with ZIKV on day 7 after birth, which may be due to direct cytopathic effects or immune-mediated olfactory damage induced by ZIKV infection.

Methods

Ethics

All studies with infectious ZIKV were performed under biosafety level 2 (BSL-2) conditions at the Beijing Institute of Microbiology and Epidemiology. All work related to human samples was approved by the ethics committee of the Seventh Affiliated Hospital of Sun Yat-sen University, Shenzhen (No. 0720) and the ethics committee of Shenzhen Institutes of Advanced Technology, Chinese Academy of Sciences (SIAT-IRB-200215-H0415). Written informed consent was obtained from all participating patients. All animal experiments were performed in a BSL-2 facility and in strict accordance with the guidelines set by the Chinese Regulations of Laboratory Animals and Laboratory Animal-Requirements of Environment and Housing Facilities. All animal experiments were approved by the Animal Experiment Committee of Laboratory Animal Center, AMMS, China (IACUC-DWZX-2020-018) and complied with the ARRIVE (Animal Research: Reporting of *In Vivo* Experiments) guidelines (https://arriveguidelines.org).

Cells and viruses

Aedes albopictus C6/36 cells (ATCC CRL-1660) were maintained in RPMI-1640 medium supplemented with 10% fetal bovine serum (FBS) (Gibco), 100 U/ml penicillin and 100 μg/mL streptomycin (Gibco) at 28 °C in 5% CO_2. BHK-21 [C-13] cells (Syrian golden hamster kidney fibroblasts, ATCC CCL-10) were cultured in Dulbecco's minimal essential medium (DMEM; Thermo Fisher Scientific, USA) supplemented with 10% FBS (Gibco), 100 U/ml penicillin and 100 μg/mL streptomycin (Gibco) at 37 °C in 5% CO_2. These two cell lines were validated in our previous study.[61] ZIKV strain GZ01 (GenBank accession No. KU820898) was originally isolated from the urine sample of a Chinese patient returning from Venezuela in 2016.[62] Viral stocks were propagated in C6/36 cells, and culture supernatants containing ZIKV were collected at 5 days post-inoculation. BHK-21 cells were used for the determination of virus titers by a plaque formation assay.

Generation of human olfactory organoids

Human olfactory mucosal air-liquid interface (ALI) cultures were derived from three residual patient biopsy samples. These three samples were originated from an 11-year-old male, a 55-year-old middle-age male and a 63-year-old senior female suffered from chronic rhinosinusitis with nasal polys, respectively. The olfactory mucosal epithelium was located by the surgeon and obtained from the upper region of the nasal cavity of patients subjected to radical endoscopic sinus surgery. The obtained tissue was then washed with sterile PBS, dissected to obtain the healthy epithelial portion of the tissue, and cut into small pieces using sterile scissors. The tissue pieces were then enzymatically digested by Dispase I (Stemcell Technologies, CA), centrifuged to purify the cell portion, plated in culture dishes with 3T3 fibroblast cells as feeder cells, and expanded using PneumaCultTM-Ex Plus Medium (Stemcell Technologies, CA). After progenitor cell expansion, the cultured cells were transferred onto 0.4 μm Transwell chambers (Corning transwell 3470) on a 24-well plate and differentiated in ALI culture using PneumaCultTM-ALI Medium (Stemcell Technologies, CA).

Mouse experiments

The strains of mice used in this study were ICR (CD-1), AG6 (IFN-α/β and IFN-γ receptor knockout mice) and A129 (IFN-α/β receptor knockout mice). ICR mice were purchased from Beijing Vital River Laboratory Animal Technology Co., Ltd. AG6 and A129 mice were bred by the Laboratory Animal Center of Academy of Military Medical Science (AMMS). All of the mice were housed and maintained in microisolator cages under pathogen-free conditions in the animal facility of the animal center of AMMS. A total of 149 animals were used in this study. No animals were excluded from this study. The experimental mice were randomly allocated to each group but confounders were not controlled. All caretakers and technicians were blinded to group allocation. The experimental design and the outcome measures were summarized in Figs. 1 and 2.

For neonatal mouse experiments, groups of three-day-old ICR suckling mice were inoculated with 10^3 PFU of virus or the same volume of PBS intracerebrally (i.c.) route, and OE, OB and brain tissues were collected at 2, 4, 6 or 8 dpi (n = 3 per group) and subjected to viral detection. For the olfactory function test, two groups of seven-day-old ICR suckling mice were inoculated with 10 PFU ZIKV or equal volume of PBS (control) via i.c. route (n = 33 per group) and raised together with their mother and littermates until weaning at postnatal day 26. Animals were monitored daily for their survival rate, weight loss and clinical symptoms until 42 days post-inoculation. The olfactory behavior test was performed on survival mice at 28, 35 and 42 dpi.

For the A129 or AG6 mouse experiments, groups of mice were infected with 10^4 PFU (AG6) or 10^5 PFU (A129) of virus by intranasal (i.n.) injection. Mock-treated mice were administered an equal volume of PBS via the same route. For the establishment of infection models, groups of 10 (AG6) and 12 (A129) animals were used and monitored daily for survival rate, weight loss and clinical symptoms. For viral RNA detection, serum samples and various tissues were collected at the indicated time points. RE, lung, OE, OB and brain tissues were isolated and weighted as previous described,[63,64] and stored at –80 °C until RNA extraction and quantitative real-time PCR (qRT–PCR) analyses (n = 3 per group). In addition, the brains of the mice were dissected and fixed in 4% paraformaldehyde (PFA) fixative solution for paraffin embedding and further detection.

ZIKV-specific IgG detection

The serum samples were tested for IgG antibodies against ZIKV by enzyme-linked immunosorbent assay (ELISA) as previous described.[65] Briefly, 96-well polysorb enzyme-linked immunosorbent assay plates (Nunc, USA) coated with 100 ng per well concentration of recombinant ZIKV envelope protein (Cat: 40543-V08B4, Sino Biological, Beijing, China) were used. Plates were blocked in 5% (vol/vol) bovine serum albumin in 1 × PBS for 1 h at 37 °C, then washed thrice with PBST (1 × PBS with 0.05% Tween-20). The serially diluted serum samples were added to each well of the plates and incubated for 1 h at 37 °C. After washing the plates with PBST, a suitable concentration of mouse IgG antibody was added to each well for 1 h at 37 °C. 3, 3′, 5, 5′-tetramethylbenzidine (TMB) (Solarbio, China) was used as substrate and the reaction was terminated using 2.0 M H_2SO_4. The optical density (OD) was measured using a microplate reader (Beckman, USA) at 450 nm and the cut off was set at twice the OD value of the control serum.

Buried food pellet test

Olfactory function was evaluated by the standard buried food pellet test (BFPT), as previously described.[60] Briefly, two days prior to the test, mice were subjected to food restriction by providing 0.2 g of chow pellets per mouse per day, with free access to water. On the test day, mice were habituated to the testing environment for at least 1 h to familiarize them with both the testing cage and the room. The experiment was performed in a clear test cage of a regular size (length × width × height: 45 cm × 24 cm × 20 cm) with 3-cm-high clear corncob bedding. The food pellet was located and buried 0.5 cm below the surface of the bedding at random sites in the cage during each trial. In each trial, one mouse was placed in the center of a test cage with the pellet hidden inside it, and the latency to find the food pellet was recorded when the mouse dug up and grasped the food with its forepaws or teeth within 5 min. If a mouse failed to find the food pellet within 5 min, the time was

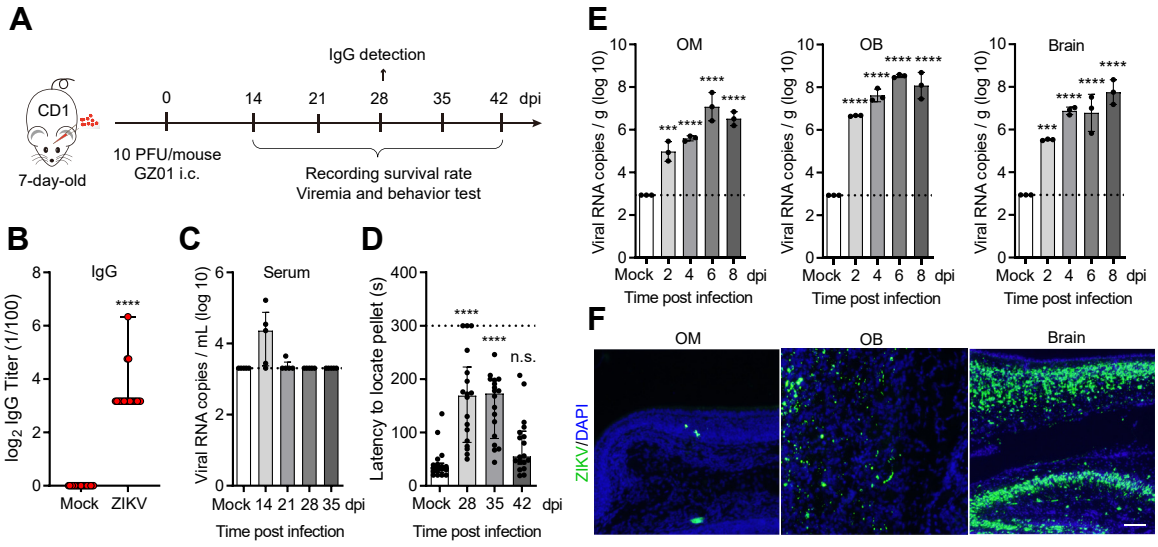

***Fig. 1:* ZIKV infection of olfactory tissues in suckling ICR mice.** (**A** to **D**) Seven-day-old ICR suckling mice were infected intracerebrally with 10 PFU of Zika virus (ZIKV) (**A**). Blood samples were collected at 28 days after ZIKV infection or mock treatment. ZIKV-specific IgG antibody was determined by ELISA plates coated with soluble ZIKV Envelope protein. (n = 21) (**B**), and serum levels of viral RNA were detected by qRT–PCR analysis (n = 5) (**C**). The olfactory function of infected and mock-treated mice was assessed by a buried food pellet test 4–6 weeks post-infection and 4 weeks post inoculation, respectively (n = 18) (**D**). Data are presented as median and interquartile range and were analyzed using Mann Whitney U test (B) and Kruskal–Wallis with Dunn's multiple comparisons test (C, D). (**E** and **F**) Three-day-old ICR suckling mice were infected intracerebrally with 10^3 PFU of ZIKV, mice were sacrificed at different time points, the OM, OB and brain tissues (n = 3) were collected to analyze ZIKV RNA levels by qRT–PCR analysis (**E**) and viral loads by *in situ* RNAscope hybridization, Scale bar, 50 μM (**F**). The limit of detection (LOD) is indicated by the dotted line. The data are presented as the mean ± SD and were analyzed with Ordinary one-way ANOVA test. p values are indicated by ***, p < 0.001; ****, p < 0.0001.

recorded as 5 min. After recording, the mice were allowed to consume the food pellet and then placed back in their home cages.

RNA extraction and quantitative real-time PCR (qRT–PCR) analyses

The viral RNA levels were determined by qRT–PCR, as described previously. Briefly, total RNA was extracted from the individual tissues using TRIzol reagent (Invitrogen, Carlsbad, CA, USA) according to the manufacturer's instructions. The total RNA of serum was isolated using the PureLink RNA Mini Kit (Cat: 12183018A, Invitrogen, Carlsbad, CA, USA) and eluted in 60 μl of RNase-free water. ZIKV RNA was measured with the ZIKV-specific primer-probe set: ZIKV-SAF (5′-GGTCAGCGTCCTCTCTAATAAACG-3′), ZIKV-ASR (5′-GCACCCTAGTGTCCACTTTTTCC-3′) and ZIKV-Probe (5′-FAM-AGCCATGACCGACAC CACACCGT-BHQ1-3′). qRT–PCR was performed using a One Step PrimeScript RT–PCR Kit (Takara Bio, Otsu, Japan) with the LightCycler® 480 System (Roche Diagnostics Ltd, Indianapolis, Indiana, USA). The following cycling conditions were applied: 42 °C for 5 min, 95 °C for 10 s, followed by 40 cycles of 95 °C for 5 s and 60 °C for 20 s. The absolute quantification of ZIKV RNA levels was calculated by using the standard curve generated from ZIKV RNA transcripts. Each sample was assayed in triplicate.

RNAscope ® *in situ* hybridization (ISH) and immunofluorescence assay (IFA)

For the ZIKV genomic RNA detection *in situ*, RNAscope *in situ* hybridization (ISH) was performed using an RNAscope 2.5 HD Assay Kit-BROWN (Advanced Cell Diagnostics (ACD), Newark, CA, USA) and ZIKV RNA specific probe (RNAscope probe-V-ZIKVsph2015) according to the manufacturer's manual. Tissue sections (2.5 μM thick) were deparaffinized in xylene and rehydrated in an ethanol series. Endogenous peroxidase activity of the tissue sections was blocked with hydrogen peroxide for 10 min before pretreatment with boiling in 1 × RNAscope target retrieval buffer (ACD, Cat No.: 322000) in a water bath for 15 min. After treatment with protease plus (ACD, Cat No.: 322330) in a HybEZ oven for 30 min at 40 °C, slides were detected using a 2.5 HD Reagent Kit (Brown) (Cat No.: 322310) and RNAscope probe-V-ZIKVsph2015 (Cat No.: 467871) and then counterstained with hematoxylin. Images were obtained with a Pannoramic DESK, P-MIDI, P250, P1000 (3D HISTECH; Hungary) and were observed with a Pannoramic Scanner (3D HISTECH; Hungary).

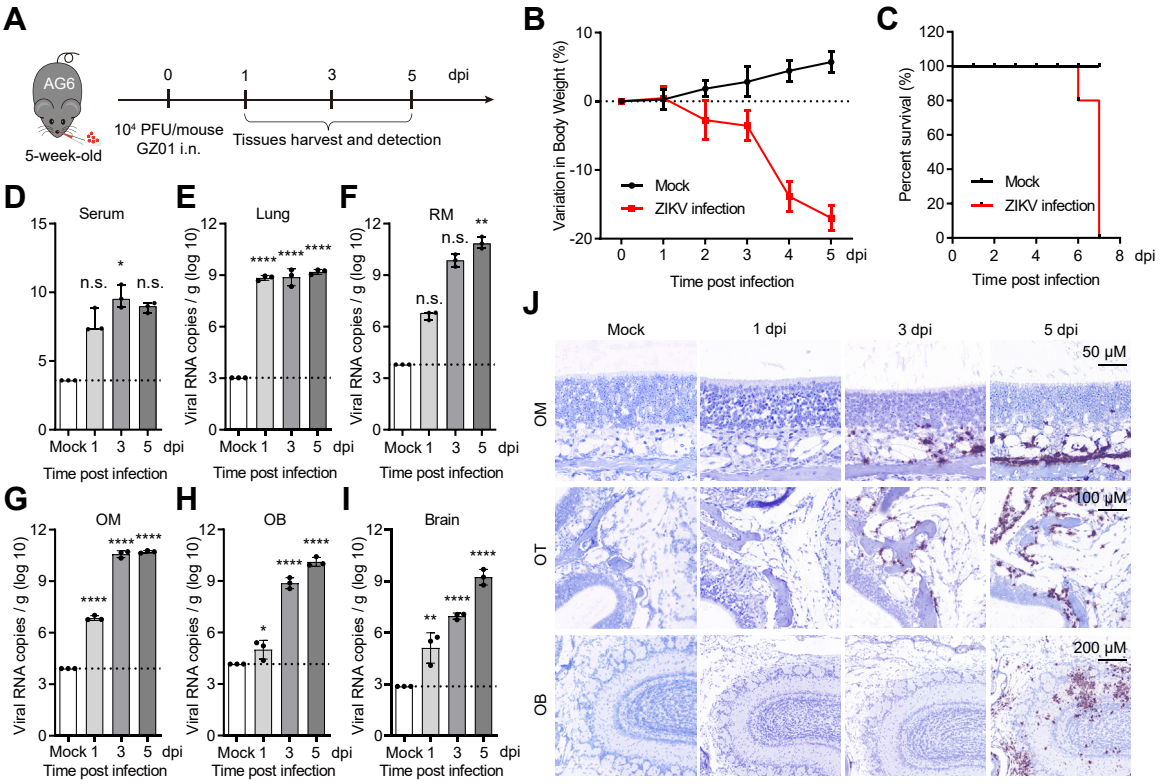

Fig. 2: **ZIKV infection in the olfactory system of AG6 mice.** (**A**) Overview of the experimental design used to evaluate infection of the olfactory system in AG6 mice after intranasal (i.n.) administration of ZIKV. Five -week-old AG6 mice were intranasally infected with 10^4 PFU of ZIKV. Mice were euthanized and dissected at 1, 3 and 5 dpi for virus detection. (**B** and **C**) The survival rate and body weight were recorded. (**D** to **F**) ZIKV RNA copies were detected in the serum (D), lung (E) and RM (F) by real-time qPCR and are shown as median and interquartile range (D, F) or the mean ± SD (E) from three independent replicates. Data were analyzed using Kruskal–Wallis with Dunn's multiple comparisons test (D, F) or one-way ANOVA with Dunnett's multiple comparisons tests (E). (**G** to **I**) ZIKV RNA copies were detected in olfactory tissues (OM, OB) (G, H) and the brain (I) by real-time qPCR and are shown as the mean ± SD from three independent replicates. Data were analyzed using one-way ANOVA with Dunnett's multiple comparisons tests. The limit of detection (LOD) is indicated by the dotted line. (**J**) The tissue distribution of viral RNA was determined in the OM, OT and OB with probe-based RNAscope *in situ* hybridization (ISH) technology. Scale bars, 50 μM, 100 μM and 200 μM. p values are indicated by *, $p < 0.05$; **, $p < 0.01$; ****, $p < 0.0001$.

To detect replication of the ZIKV genome, the tissue sections were stained following an RNAscope Fluorescence Assay with a RNAscope Multiplex Fluorescent Reagent Kit v2 (Cat No.:323100) and ZIKV negative-sense RNA specific probe (RNAscope Probe-V-ZIKV-NS3-sense (Cat No.: 1073501)). For codetection of ZIKV RNA and olfactory cell marker proteins, a combination of an RNAscope Fluorescence Assay with an immunofluorescence assay (IFA) was performed by using RNAscope Probe-V-ZIKV-NS3-sense (Cat No.: 1073501) and several cell marker antibodies, including anti-S100beta (S100B, olfactory ensheathing cell marker) (Abcam, Cat No.: ab52643), anti-olfactory marker protein (OMP, mature olfactory receptor neuron marker) (Abcam, Cat No.: ab183947), anti-GAP43 (immature olfactory receptor neuron marker) (Abcam, Cat No.: ab5220), anti-Cytokeratin 8 (CK8, sustentacular cell and Bowman's gland marker) (Abcam, Cat No.: ab53280), and anti-Cytokeratin 5 (CK5, horizontal basal cell marker) (Abcam, Cat No.: ab52635), following fluorescent tyramide-signal amplification (TSA)-based procedures. All the antibodies used here were validated in our previous study.[63] The fluorescent signals were scanned with a Pannoramic DESK, P-MIDI, P250, P1000 (3D HISTECH; Hungary) and observed with a Pannoramic Scanner (3D HISTECH; Hungary).

Histopathology assay

For histopathology analyses, tissues dissected from the experimental mice were fixed in 4% PFA and sectioned into 2.5 μM-thick section slices. After being deparaffinized in xylene and rehydrated in a graded alcohol series, the paraffin sections were stained with hematoxylin and eosin (H&E) according to standard procedures. All sections were scanned with a Pannoramic DESK, P-MIDI, P250, P1000 (3D HISTECH; Hungary) and

were observed with a Pannoramic Scanner (3D HISTECH; Hungary). Damage parameters of OM and OB in the sections was scored semiquantitatively (OM: structural damage, edema, inflammation cell infiltration and abnormal mucus secretion; OB: structural damage, edema, inflammation cell infiltration and hemorrhage), none = 0, mild = 1, moderate = 2, and severe = 3; total maximum score = 12. The total scores were summed and divided by the number of animals for each group to get the group mean score. Scoring was performed by a pathologist blinded to sample numbers.

Luminex assay

For the measurement of cytokines and chemokines in the olfactory tissues and serum derived from A129 mice, the OE and OB were dissected from the experimental mice, and the total protein was extracted using radioimmunoprecipitation assay (RIPA) lysis buffer (CWBIO, Cat No.: CW2334S). Whole blood samples from mice were collected through the ophthalmic venous plexus and allowed to clot for 1 h at room temperature. Then, the serum was collected by centrifugation at 2500 rpm for 10 min. Cytokines and chemokines were measured using the Cytokine & Chemokine 36-Plex Mouse ProcartaPlex™ Panel 1A (Cat No.: EPX360-26092-901, Invitrogen, CA, USA) according to the manufacturer's instructions. Each sample was analyzed in triplicate. The data were measured using a Luminex-200 system and the XMap Platform (Luminex Corporation, Austin, TX, USA).

RNA library construction and sequencing

OM and OB tissues from mock-treated and ZIKV-infected AG6 mice were collected for RNA-Seq. Total RNA from these tissues was extracted using TRIzol reagent (Invitrogen, Carlsbad, CA, USA) and Dnase I (NEB, USA). Sequencing libraries were generated using the NEBNext® UltraTM RNA Library Prep Kit for Illumina® (#E7530 L, NEB, USA) following the manufacturer's recommendations, and index codes were added to attribute sequences to each sample. The clustering of the index-coded samples was performed on a cBot cluster generation system using HiSeq PE Cluster Kit v4-cBot-HS (Illumina, San Diego, California, USA) according to the manufacturer's instructions. After cluster generation, the libraries were sequenced on an Illumina Novaseq6000 platform, and 150 bp paired-end reads were generated. After sequencing, fqtools_plus (github.com/annoroad/fqtools_plus) was used to filter the original data (raw data) to clean reads by removing adapter-contaminated reads and low-quality reads. Clean reads were aligned to the mouse genome (Mus_musculus.GRCm38.99) using HISAT2 v2.1.0. The number of reads mapped to each gene in each sample was counted by HTSeq v0.6.0, and TPM (transcripts per kilobase of exon model per million mapped reads) was then calculated to estimate the expression levels of genes in each sample.

Genes with Padj < 0.05 and $|\text{Log2FC}| \geq 1$ were identified as Differentially Expressed Genes (DEGs). DEGs were used as queries to search for enriched biological processes (Gene Ontology BP) using Metascape. Heatmaps of gene expression levels were constructed using the heatmap package in R (https://cran.rstudio.com/web/packages/pheatmap/index.html). Dot plots and volcano plots were constructed using the ggplot2 (https://ggplot2.tidyverse.org/) package in R.

Statistics

To determine the group size in ZIKV infection experiments, statistical power analysis was made based on data from previous studies.[66–68] We assumed that ZIKV infection causes 25% (ICR), 100% (AG6) and 50% (A129) mortality in mice, and the mortality rates of mice in mock-treated groups are 0%. The difference of survival rate between ZIKV-infected group and mock-treated group is considered as effect size. The power analyses were performed at 5% of significance level and 80% power using the following formula published previously[69]: Sample size $= 2 (Z^{a}_{/2} + Z^{\beta})^2 \times P (1 - P)/(p_1 - p_2)^2$. According to the power analysis, at least 27 (ICR), 4 (AG6) or 11 (A129) mice per group were needed. All quantifications and analyses were done by investigators blinded to treatment conditions. Data were analyzed using GraphPad Prism 8 (GraphPad Software, San Diego, California, USA). Depending on the results of Gaussian distribution analyses with Shapiro–Wilk test, Student's t tests, Ordinary one-way ANOVA analysis of variance with Dunnett's multiple comparisons correction or nonparametric Mann–Whitney U test and Kruskal–Wallis with Dunn multiple comparison correction tests were used. The values shown in the graphs are presented as the mean ± SD or median and interquartile range of at least three independent experiments. $p < 0.05$ was considered to indicate statistical significance. p values are indicated by *, $p < 0.05$; **, $p < 0.01$; ***, $p < 0.001$; and ****, $p < 0.0001$.

Role of funders

The funders did not have any role in study design, data collection, data analyses, interpretation or writing of the report.

Results

Subtle olfactory dysfunction was observed in adolescent ICR mice after neonatal ZIKV infection

To investigate the olfactory consequences and progression of ZIKV infection in the olfactory system after neonatal infection, we used an immunocompetent ICR (CD-1) neonatal mouse model with intracerebral inoculation of ZIKV (Fig. 1A). To investigate the changes in olfactory function after ZIKV infection, 7-day-old ICR mice were infected with GZ01 intracerebrally at a dose of 10 PFU/mouse, and approximately 34% of the mice

died within 21 days post-infection (dpi) (Fig. S1A). ZIKV infection induced high levels of ZIKV-specific IgG antibodies in the serum on day 28 post-infection, indicating successful infection with ZIKV in the experimental group (Fig. 1B). We randomly chose 5 out of 21 surviving mice for the evaluation of viremia on days 21, 35 and 42 post-infection. A low level of viral RNA ($10^{3.65}$ copies/mL) in the serum was detected at 21 dpi in one surviving mouse, but viral RNA was at the limit of detection in the remaining mice (Fig. 1C). Regarding the duration of infection, viremia was completely cleared from the serum one to three weeks later (28 dpi to 42 dpi) in all surviving mice (Fig. 1C). After maternal ablactation, the well-established buried food pellet test (BFPT) was carried out as previously described to assess the olfactory sensitivity of pups.[63] Mice were given a restricted diet (0.2g chow/mouse/24 h) for 2 days before testing and during the experimental period. The olfactory behavior test was performed on weaning mice at 28-, 35- and 42 dpi. We observed a significant latency to find the food pellet in the infected mice compared with the mock-treated group at 28 dpi ($p < 0.0001$), and this difference was maintained until 35 dpi ($p < 0.0001$), when a slight recovery was observed. Moreover, approximately 16.67% of infected mice (3 out of 18) had dysosmia (failed to find the food pellets within 300 s) at 28 dpi. Complete recovery of olfactory function was observed at 42 dpi ($p = 0.1646$) (Fig. 1D). Infection-related damage to olfactory function may be caused by the direct infection of the olfactory system by ZIKV.

To verify our hypothesis, 3-day-old ICR mice were intracerebrally infected with ZIKV for the evaluation of ZIKV infection in olfactory tissues. OM, OB, brain and other tissues were dissected for the detection of ZIKV RNA levels and localization of infection by qRT–PCR and *in situ* hybridization (ISH) with ZIKV-specific probes. ZIKV exhibited broad tropism and replicated in several tissues, including the RM lining of the upper respiratory tract (Fig. S1B). Consistent with previous studies, substantial amounts of viral RNA were observed in the brain, with a continual increase over time (Fig. 1E), and abundant viral RNA was detected in the cerebral cortex and hippocampus and other regions in the brains of neonatal mice at 8 dpi (Fig. 1F). In the olfactory system, high levels of viral RNA were detected in the OB of the central nervous system (Fig. 1E) at 2, 4, 6 and 8 dpi with a broad distribution at 8 dpi (Fig. 1F). Moreover, lower levels of viral RNA were detected in the OM within the peripheral nervous system using qRT–PCR, and a small amount of ZIKV RNA was also detected *in situ* in the OM via RNAscope hybridization (Fig. 1E and F), indicating susceptibility to ZIKV in both OB and OM tissues.

The olfactory tissues were susceptible to ZIKV infection in AG6 mice

To further investigate ZIKV susceptibility and infection dynamics in olfactory tissues, 5-week-old AG6 mice (interferon-α/β and interferon-γ receptor deficient) were inoculated intranasally with 10^4 PFU of the ZIKV GZ01 strain (Fig. 2A). Similar to our previous study,[61] AG6 mice succumbed ZIKV infection via the i.n. route, with continuous body weight loss (Fig. 2B and C) and a high viral load in both the serum and lung (Fig. 3D and E). Additionally, a high level of viral RNA was observed in the RM of AG6 mice as early as 1 dpi, with a continuous increase at 3 dpi and 5 dpi (Fig. 2F), and we also observed the *in situ* distribution of viral RNA in the RM at 3 dpi and 5 dpi (Fig. S2A).

In the olfactory system, viral RNA was persistently detected in the OM and OB at 1–5 dpi, with the highest viral loads of $10^{10.71}$ copies/g (OM) and $10^{10.12}$ copies/g (OB) at 5 dpi (Fig. 2G and H). By using the specific probe of ZIKV genomic RNA, RNAscope probe-V-ZIKVsph2015, ZIKV RNA was first detected *in situ* in the OM via RNAscope at 3 dpi, and robust ZIKV RNA signals were also detected in the OM at 5 dpi (Fig. 2J). Simultaneously, we detected viral RNA signals located in the olfactory tract (OT) of olfactory nerve fibers at 3 dpi and 5 dpi, the fibers extend from the OM and project through the cribriform plate (CP) to the OB of the CNS (Fig. 2J). However, no ZIKV RNA was detected *in situ* in the OB until 5 dpi (Fig. 2J), indicating delayed replication of ZIKV in the OB compared to the OM and OT. In addition, a strong ZIKV RNA signal was detected in the olfactory cortex (region of the brain responsible for receiving and processing sensory signals) at 5 dpi (Fig. S2B). Additionally, to determine whether ZIKV could actively replicate in the olfactory tissues, RNAscope probe-V-ZIKV-NS3-sense targeting the reverse complement sequence of ZIKV was used to detect the replication intermediates, ZIKV negative-sense RNA, *in situ*. Consistent with the distribution of ZIKV genomic RNA, we also noted the fluorescence signals of the negative-sense RNA in OM, OT (at 3 dpi and 5 dpi) and OB (at 5 dpi) (Fig. S2D). Taken together, our results indicated that ZIKV could infect and replicate effectively in the olfactory system of AG6 mice.

ZIKV mainly targets olfactory ensheathing cells and induces pathological damage in both the olfactory mucosa and olfactory bulb of AG6 mice

The olfactory mucosa is a pseudostratified columnar epithelium and consists of several distinct cell types including neuroepithelial cells (mature and immature olfactory sensory neurons (mOSNs, iOSNs) and OECs), non-neuroepithelial cells (sustentacular cells, microvillar cells and Bowman's duct and gland cells) and olfactory stem/progenitor cells (basal cells). To determine the target cell types of ZIKV in the OM of AG6 mice, an RNAscope fluorescence assay of viral replication based on negative-sense template RNA combined with an immunofluorescence assay (IFA) of olfactory markers was performed with the ZIKV negative-sense probe and specific cell markers. Notably, substantial expression of

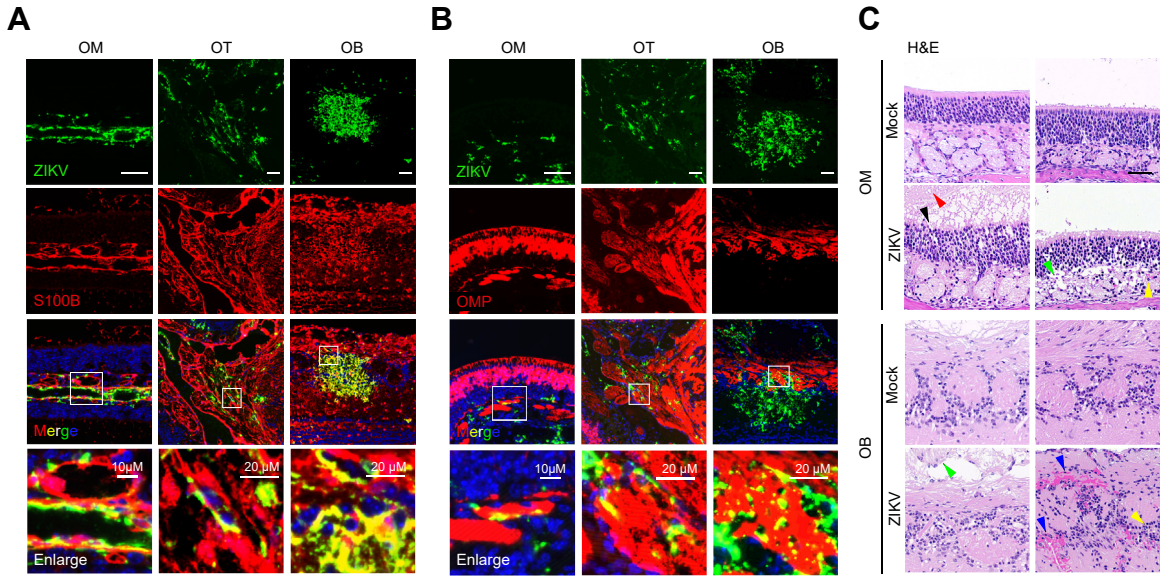

***Fig. 3*: ZIKV primarily targeted neuroepithelial cells and resulted in pathological injury in OM and OB tissues from AG6 mice.** (**A** and **B**) Multiplex immunofluorescence detection showing the colocalization between ZIKV negative-sense RNA and the S100B protein (a marker of OECs) (A) or the OMP protein (a marker of mature olfactory sensory neurons) (B) in the OM, OT and OB. Scale bar, 50 μM. (**C**) Representative hematoxylin and eosin (H&E) staining of the OM and OB tissues from AG6 mice revealed the histopathological changes caused by ZIKV infection. Pathological injury is indicated by colored arrows (epithelial cell loss, black arrow; abnormal mucus secretion, red arrow; edema, green arrow; neutrophil infiltration, yellow arrow; hemorrhage, blue arrow). Scale bar, 50 μM.

viral RNA was detected in the OT lining in the lamina propria (LP) of the OM, which consists of olfactory neurons and OECs. According to the colocalization of ZIKV RNA and specific cell markers, we found that ZIKV infection occurred in multiple S100B$^+$ OECs in the OM (Fig. 3A). Additionally, substantial ZIKV infection was also detected in the S100B$^+$ OECs in the OT that pass through the olfactory cribriform plate of ethmoid bone and the outer nerve layer of the OB (Fig. 3A). Simultaneously, a small proportion of OMP$^+$ mOSNs in the OM, OT and OB were also infected with ZIKV (Fig. 3B), indicating the neurotropism of ZIKV in olfactory tissues. Moreover, we also detected the colocalization of ZIKV negative-sense RNA with the GAP43, CK8 and CK5 proteins (Fig. S3A), which revealed that iOSNs, sustentacular cells and horizontal basal cells were also target cells of ZIKV infection.

Furthermore, the changes in histopathology of OM and OB induced by ZIKV infection were characterized by hematoxylin and eosin (H&E) staining. Notably, ZIKV infection resulted in mild structural damage to the OM, which presented as irregularly arranged cells in the olfactory epithelium, loss of a small number of epithelial cells and slight edema of the LP, as well as moderate neutrophil infiltration of the OM and abnormal mucus secretion in the nasal cavity. Additionally, ZIKV infection resulted in slight edema, neutrophil infiltration and hemorrhage in the OB (Fig. 3C and Fig. S3B). The mild injury and inflammation in the OM and OB caused by ZIKV infection may contribute to transient olfactory dysfunction in mice.

ZIKV infection induces robust immune responses and substantial dysregulation of host genes in AG6 mice

To comprehensively investigate the cellular response induced by ZIKV infection in olfactory tissues at the molecular level, we carried out global transcriptome analyses of mouse OM and OB infected with ZIKV in comparison with the mock-treated group. OM and OB tissues were isolated from mock treated and ZIKV infected AG6 mice following total RNA extraction and Cdna library construction. Principal-component analysis (PCA) discriminated mock-infected controls from ZIKV-infected OM/Obs based on the expression levels of genes. Compared with 3 dpi, at 5 dpi, both the OM and OB showed substantial differences from mock-infected controls (Fig. 4A). Genome-wide analysis identified 273 DEGs, including 239 significantly upregulated and 34 significantly downregulated genes, in ZIKV-infected OM at 3 dpi compared with the mock-treated OM (Fig. S4A and B). At 5 dpi, the number of dysregulated genes significantly increased, with 746 upregulated genes and 425 downregulated genes, which may be due to the increased viral load at 5 dpi compared to 3 dpi (Fig. 4B). In OB tissues, we also detected a small number of differentially expressed genes at 3 dpi

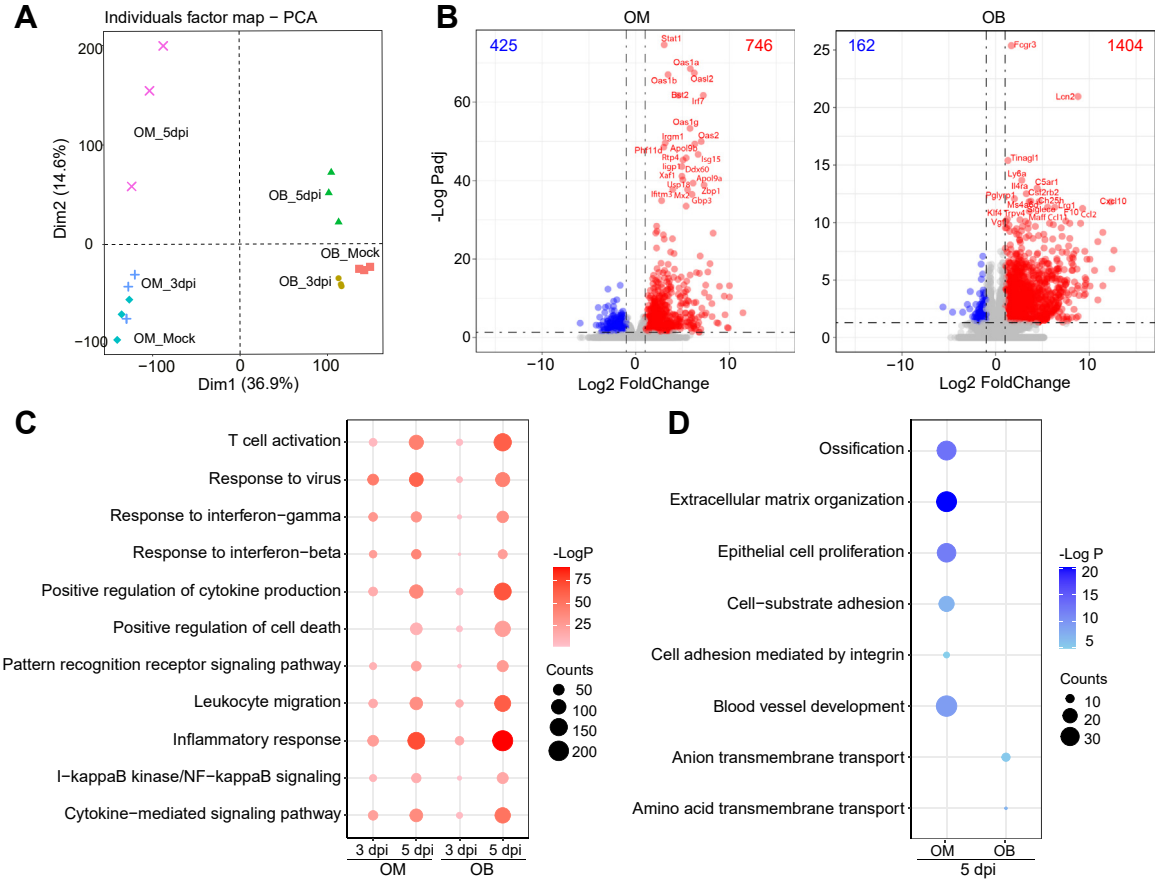

Fig. 4: **Comparison of dysregulated genes associated with ZIKV infection in the OM and OB of AG6 mice.** (**A**) Principal-component analysis (PCA) of the global transcriptomic data in mock- (n = 3) and ZIKV-infected (n = 3) OM/OB at 3 and 5 days post-infection. (**B**) Volcano plots indicating differentially regulated genes in the OM and OB at 5 days post-ZIKV infection. Significantly upregulated genes (padj < 0.05 and fold change ≥ 2) are colored red; significantly downregulated genes (padj < 0.05 and fold change ≥ 2) are colored blue; others are colored gray. The top 20 upregulated genes are marked with gene symbols. (**C** and **D**) Dot plot visualization of enriched GO terms of upregulated genes (C) and downregulated genes (D) in the OM and OB at the indicated time points.

(122 upregulated genes and 14 downregulated genes) and a large number of dysregulated genes at 5 dpi (1404 upregulated genes and 162 downregulated genes) (Fig. S4A and B, Fig. 4B). Genes involved in IFN responses including Stat1, Oas1a, Oas1b, Oasl2, Isg15, Zbp1, and Ifitm3, were among the most significantly upregulated genes in the OM at 5 dpi. In the OB, the expression levels of cytokines including Ccl2, Ccl11 and Cxcl10 were greatly increased. An ISG, Ch25h, was among the top 10 upregulated genes in the OB (Fig. 4B).

Gene ontology (GO) enrichment analysis indicated that the major upregulated genes in the OM and OB in response to ZIKV infection were related to the antiviral response including the immune response and inflammatory response at both 3 dpi and 5 dpi (Fig. 4C). The downregulated genes were associated with epithelial cell organization-, proliferation- and integrin-related pathways and mostly occurred in the OM at 5 dpi, indicating that ZIKV infection may induce disorganization of the OM structure (Fig. 4D). In both the OM and OB, many genes related to cytokine-mediated signaling pathways were upregulated, with Ifna4, Ifnb1, Ifng and several chemokines being the most significantly altered genes. Additionally, genes involved in cell death were significantly upregulated in the ZIKV-infected OM and OB, these genes included Il6, Tnf, S100a8 and S100a9, which had the largest fold changes (Fig. S4C and D). ZIKV infection associated cell death may be a potential cause of olfactory dysfunction.

ZIKV infects the olfactory system and induces a strong cytokine/chemokine response in OM and OB tissues from A129 mice

The susceptibility of the olfactory system to ZIKV infection was confirmed in A129 mice (interferon-α/β receptor deficient). Five to six-week-old A129 mice were

challenged with 10^5 PFU of the ZIKV GZ01 strain per mouse via the i.n. route, body weight changes and survival rates were calculated (Fig. 5A and B), and viral RNA was monitored in the serum and indicated tissues at 2, 4 and 6 dpi. ZIKV viral RNA maintained high levels in the serum at both 2 dpi and 4 dpi, and reached its highest levels in the RM and lung at 4 dpi (Fig. 5C). Besides, higher viral RNA levels were detected in OM and OB at 4 dpi and 6 dpi, and lower viral RNA levels were also detected in the brain (Fig. 5E), indicating susceptibility to ZIKV in the olfactory tissues of A129 mice. The above results were confirmed by RNAscope ISH technology (Fig. 5D and F). Over all, these results indicated that olfactory system infection and effective viral replication of ZIKV could also be established via i.n. in A129 mice.

To characterize the immune activation in the olfactory system after ZIKV infection via the i.n route, we assessed the expression levels of 36 cytokines in OM and OB tissues from ZIKV-infected and mock-treated A129 mice at 2-, 4- and 6 dpi on the Luminex Xmap platform using a 36-plex mouse cytokine and chemokine panel. In the OM, the concentrations of 9 cytokines/chemokines increased at different time points in the ZIKV-infected mice in comparison with the mock-treated controls (Fig. S5A and B). Among these cytokines, the concentrations of the proinflammatory cytokine IL-1β and the chemokine MIP-1α/CCL3 showed gradually increased within 6 days of ZIKV infection. Three cytokines showed upregulated expression at 4 dpi, including the proinflammatory cytokines TNF-α, the anti-inflammatory cytokine IL-10 and the chemokine MCP-3/CCL7, among which CCL7 remained upregulated at 6 dpi. Additionally, the increase in the levels of four cytokines including interferon IFN-γ and chemokines CCL5, IP-10/CXCL10 and IL-15, occurred only at 6 dpi. We also observed upregulated levels of 9 cytokines/chemokines in the OB from ZIKV-infected mice, including the interferons IFNγ, the proinflammatory cytokines IL-12p70, IL22, IL-6, IL-18, and LIF and the

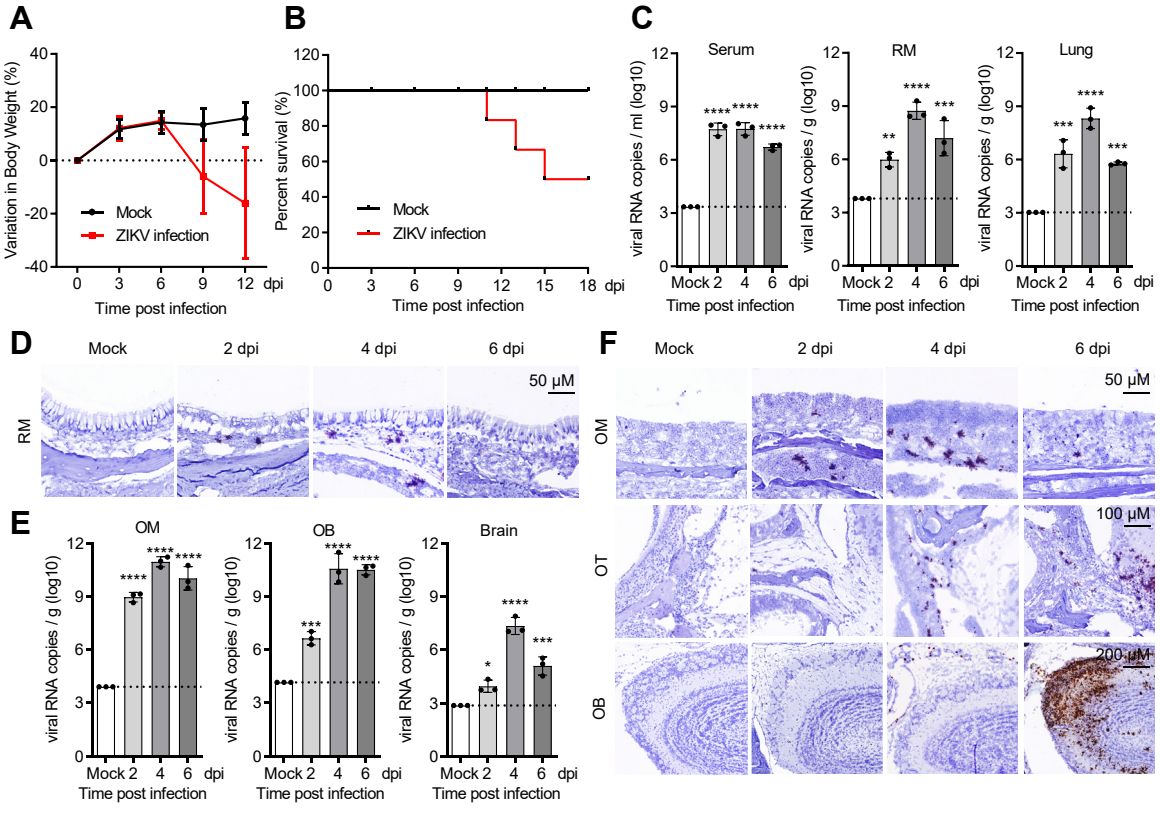

***Fig. 5:* The olfactory system and respiratory tissues were vulnerable to infection with ZIKV in A129 mice.** Five-to six-week-old A129 mice were intranasally infected with 10^5 PFU of ZIKV. (**A** and **B**) Body weight changes (A) and survival rates (B) were monitored. Mice were euthanized and dissected at 2, 4 and 6 dpi for virus detection. (**C** and **E**) ZIKV RNA copies were detected in the RM, lung, serum (C), OM, OB and brain (E) by real-time qPCR and are shown as the mean ± SD from three independent replicates. Data were analyzed using one-way ANOVA with Dunnett's multiple comparisons tests. p values are indicated by *, $p < 0.05$; **, $p < 0.01$; ***, $p < 0.001$; ****, $p < 0.0001$. (**D** and **F**) The tissue distribution of viral RNA was determined in the RM (D), OM, OT, and OB (F) with probe-based RNAscope *in situ* hybridization (ISH) technology. Scale bars, 50 μM, 50 μM, 100 μM and 100 μM.

chemokines CCL2, CCL7, and CCL5; all of the increased cytokine expression occurred at 6 dpi (Fig. S5A and B), indicating delayed ZIKV infection in the OB compared to the OM in infected mice. Thus, multiple cytokines were induced following ZIKV infection in the OM and OB, which is consistent with the results of the transcriptome analyses above, suggesting that cytokines may play crucial roles in the viral clearance and olfactory damage during ZIKV infection.

Human olfactory organoids were permissive for ZIKV infection

In vitro culture of human organoids isolated from specific tissues provides a better human model system and has been widely used for the study of host–virus interactions including tissue susceptibility, pathogenesis of viral infection and cell tropisms in human tissues. To further investigate the susceptibility of human olfactory tissues to ZIKV infection, we developed human olfactory mucosal-derived olfactory organoid cultures using an ALI culture system. In this culture system, human olfactory mucosal tissues were digested into single primary cells, cocultured with 3T3 fibroblast feeder cells for the expansion of progenitor cells and then transferred into Transwell chambers for the differentiation of progenitor cells at the ALI (Fig. 6A). After 15–20 days of culture, the cells were differentiated into a polarized, pseudostratified mucociliary olfactory epithelial structure containing several types of olfactory epithelial cells including $CD73^+$ microvillar cells, $SOX9^+$ Bowman's duct and gland cells, $S100B^+$ OECs and $CK8^+$ sustentacular cells (Fig. 6E).

For the evaluation of ZIKV susceptibility in human olfactory organoids, the organoids were infected with ZIKV at a multiplicity of infection (MOI) of 3 by applying ZIKV stock to the apical surface in the upper compartment of the chamber for 2 h at 37 °C. Then the remaining virus particles were removed from the cell surface by washing with DPBS and the medium in the lower compartment of the chamber was replaced with fresh culture medium. Cells, the fluid used to wash the apical surface and the culture medium in the lower chamber were collected at the indicated time points. In the control group, the organoids were inoculated with the same volume of culture medium, and samples from the mock-treated group were collected at 48h post inoculation. The viral load and ZIKV distribution were evaluated by qRT–PCR and multiplex immunofluorescence staining, respectively. As shown in Fig. 6B, substantial levels of viral RNA were detected in the infected organoids at 48 h post viral infection (approximately 10^8 copies/well) (Mock vs. 48 hpi., $p < 0.0001$) and a gradual increase in intracellular viral loads was observed at 120 h post-viral infection (Mock vs. 120 hpi., $p < 0.0001$; 48 hpi. vs. 120 hpi., $p = 0.0021$) (Fig. 6B). Substantial amounts of viral RNA existed in the fluid used to wash the apical surface of organoids in the Transwell chambers (Mock vs. 48 hpi., $p < 0.0001$; Mock vs. 120 hpi., $p < 0.0001$; 48 hpi. vs. 120 hpi., $p = 0.8051$) (Fig. 6C). Additionally, lower viral loads were also detected in the culture medium in the basolateral chamber at 48 h post-infection (Mock vs. 48 hpi., $p = 0.0003$). Consistently, we also observed a gradual increase in viral load in the basolateral medium at 120 h post-infection (Mock vs. 120 hpi., $p < 0.0001$; 48 hpi. vs. 120 hpi., $p < 0.0001$) (Fig. 6D), which indicated that ZIKV could infect the organoids, be transported through the apical surface to the basolateral side of the organoids, and be released into the culture medium in the lower chamber. In addition, we observed colocalization of ZIKV antigen with the CK8 and S100B proteins (Fig. 6E), indicating that ZIKV mainly targeted sustentacular cells and OECs in human olfactory organoids.

Discussion

ZIKV has been considered a major public health threat due to its relationship with microcephaly since an outbreak of ZIKV infection in the Brazilian region in 2015. As a neurotropic flavivirus, ZIKV has a strong neurovirulence in both the CNS and PNS. With further research, more evidence has revealed the extra-microcephalic signs and symptoms of broad tissue tropism in ZIKV-infected children, including arthrogryposis, clubfoot, hearing deficiencies, and ocular abnormalities.[2,62,70–72] Using an animal model, studies have also observed motor incoordination and visual dysfunctions in ZIKV infected mice.[73] Additionally, previous studies revealed that the vaginal mucosa is a highly susceptible site of ZIKV infection; such infection resulted in IUGR of the fetus in pregnant mice.[74] Viral infection of the upper respiratory tract is a common cause of clinical olfactory dysfunction. However, whether olfactory disorder is one of the symptoms in the ZIKV affected children is still unknown. To mimic clinical perinatal ZIKV infection, we infected the neonatal ICR (CD-1) mice with ZIKV at day 7 after birth (P7) and evaluated olfactory function when the mice reached puberty. ZIKV infection did not cause significant microcephaly in the surviving mice at puberty (data not shown). Interestingly, we observed a general latency to locate the food pellets in the ZIKV-infected group with 3 out of 18 mice exhibiting olfactory loss (Fig. 1D), although complete recovery of olfactory function was observed at 42 dpi. Diseases in ZIKV-affected fetuses and newborns are more complicated, and our data implied that olfactory disorder could be a new clinical symptom of ZIKV infection and may result from direct damage caused by ZIKV infection or immune-mediated damage induced by viral infection. Long-term study and follow-up are necessary for improving prognose and early interventions for affected children.

Despite limited data, direct viral infection and accumulation in olfactory system is regarded as the main

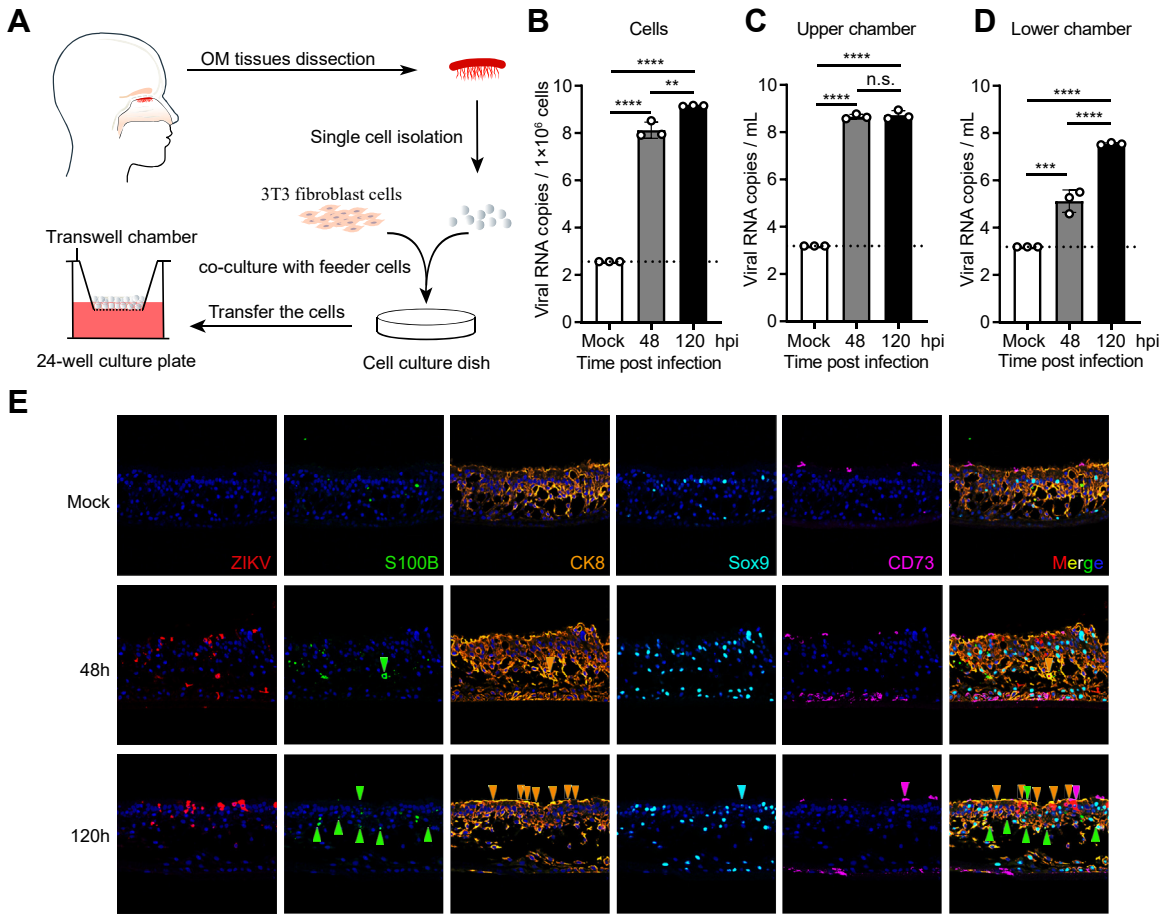

***Fig. 6:* ZIKV infection in human olfactory organoids derived from residual patient biopsy samples.** (**A**) Schematic of the strategy used for the human olfactory mucosal tissue-derived olfactory organoid culture described in detail in the methods. (**B** to **D**) Human olfactory organoids were incubated with ZIKV on the apical side at an MOI of 3. We collected the cells (B), fluid used to wash the apical surface (C) and culture medium (D) in the lower chamber at the indicated time points. Viral RNA was detected by qRT–PCR analysis. The data originated from the average value of 3 individual cultures, are presented as the mean ± SD and were analyzed by Student's t test. p values are indicated by *, $p < 0.05$; **, $p < 0.01$; ***, $p < 0.001$; and ****, $p < 0.0001$. (**E**) Representative multiplex immunofluorescence staining shows that ZIKV mainly infects S100B^{+} OECs and CK8+ sustentacular cells.

cause of PVOD.[63,75,76] To date, ZIKV susceptibility and infection dynamics in the olfactory system have rarely been studied. To verify the infection and distribution of ZIKV in the olfactory mucosa and other parts of the olfactory system within the CNS, a time-course analysis of ZIKV infection in immunodeficient mice was performed using qPCR and RNAscope ISH techniques. This allowed us to uncover the progression of the virus in AG6 mice. We showed that intranasal ZIKV inoculation in immunodeficient mice leads to robust infection of olfactory tissues with a time-dependent increase in both viral RNA and ZIKV negative-sense RNA (Fig. 2G, J and Fig. S2D), indicating an active infection in olfactory system. In accordance with the present results, Ozdener and colleagues also demonstrated that ZIKV was present in the olfactory epithelium and olfactory bulb of immunocompromised mice.[59] In accordance with our results, previous studies have suggested that the olfactory system could serve as a target of infection for neurotropic flaviviruses in addition to respiratory viruses. One early study showed that St. Louis encephalitis virus (SLE) infected the olfactory epithelium and then passed via the olfactory nerves to the olfactory lobes in infected hamsters.[57] In addition, McMinn et al. reported that Murray Valley encephalitis virus (MVE) was first detected in the olfactory lobes of footpad inoculated mice.[77] Yamada and colleagues also reported the distribution of JEV antigens in the olfactory tract and olfactory bulb of piglets.[58] To date, the olfactory system has been considered the target and neuroinvasion pathway for different flaviviruses.[53] To further validate our results, by using a relevant ex vivo model,

human olfactory organoids, we demonstrated that the human olfactory mucosa is a target for ZIKV infection. We infected primary human olfactory organoids cultured at the ALI with ZIKV apically, mimicking natural infection upon oronasal contact, and provided direct evidence that human olfactory organoids are susceptible to ZIKV infection and release virus into the basolateral chamber in a time-dependent manner (Fig. 6A–D). To our knowledge, human olfactory mucosa-derived olfactory organoids are the first ex vivo olfactory model for the study of ZIKV infection and replication and will be a valuable tool to study human-specific infection and host–virus interactions and further develop antiviral strategies.

Previously published studies have demonstrated that ZIKV can replicate in cultured human OECs.[59,78] Consistently, the data presented here show that ZIKV mainly infects S100B positive OECs in both the OM of AG6 mice and human organoids (Figs. 3A and 6E). The olfactory pathway acts as a possible shortcut for pathogens to enter the CNS, bypassing the blood–brain barrier (BBB). In the olfactory pathway, OECs wrap around olfactory sensory axons and bundle them together for the formation of olfactory nerve tracts, providing an open channel from the peripheral OM to the CNS.[79] In our study, we observed the presence of ZIKV infection in the olfactory tract crossing the cribriform plate from the OM to the CNS at 3 dpi and subsequent OB infection with ZIKV at 5 dpi (Figs. 2J and S2D). Substantial amounts of ZIKV RNA were also detected in the olfactory cortex region in addition to other parts of the CNS (Fig. S2B), which indicated that olfactory pathway is a possible route of ZIKV entry into the CNS.

In addition to direct injury by viral infection, another hypothesis about the pathogenesis of postinfectious olfactory dysfunction is inflammatory response-related damage to the olfactory system. In our study, we noted slight inflammatory infiltration of neutrophils in both the OM and OB (Fig. 3C). Simultaneously, a large number of upregulated cellular genes involved in cytokine production and cytokine-mediated signaling pathways were detected by RNA-Seq technology in response to ZIKV infection (Fig. 4C). Consistently, we noted an increase in cytokine production in ZIKV infected OMs and OBs using a Luminex assay. Among them, both pro-inflammatory (TNF-α, IP-10) and immunoregulatory (IL-10) cytokines/chemokines were upregulated in the OM (Fig. S5A and B). Most of the overexpressed cytokines/chemokines in OB display proinflammatory functions, including IFNγ, IL-12p70, IL-6, IL-18, IL-22, LIF, MCP-1/CCL2, MCP-3/CCL7, and RANTES/CCL5. The overexpression of these cytokines/chemokines may associate with both viral control and the pathogenesis of ZIKV infection in the olfactory system, indicating the significant role of inflammation in the pathogenesis of olfactory dysfunction. Additionally, ZIKV infection led to the upregulation of a large number of cellular genes involved in antiviral response and cell death and the downregulation of genes related to epithelial cell proliferation (Fig. 5C and D). This suggests that potential damage to olfactory tissues may occur after ZIKV infection and that viral infection of the olfactory system may result in clinical consequences. However, more research is needed to clarify the mechanism of pathogenesis and virus–host interactions. The comparison of our global transcriptome datasets from infected olfactory tissues with those from the mock-treated group will provide valuable resources for further investigation of the underlying cellular and molecular mechanisms and management of ZIKV-related pathological effects.

It is important to note that some limitations still present in this study. One of the limitations is that we did not investigate the relationship between ZIKV infection and olfactory disorder after maternal infection. ZIKV infection during pregnancy can be related to severe fetal outcomes and birth defects, and our results in neonatal mice indicated that olfactory dysfunction is quite possible one of sequela in human and mice after intrauterine ZIKV infection. Further study needs to be addressed to investigate our hypothesis. Another limitation is that despite animal models used in the present study are well-established tools for ZIKV infection and have shed light on the infection and pathogenesis of ZIKV in olfactory system of adult mice here, they still have inherent limits and cannot completely mimic those in humans. For example, defects in interferon pathway cause robust infection of ZIKV in immunodeficient mice, and i.c. route was used for the viral infection in neonatal ICR mice, which could not correlate well with the natural ZIKV infection in humans. In addition, although results in human olfactory organoids provided evidence that human olfactory mucosa did susceptible to ZIKV infection, whether ZIKV infection could cause olfactory damage in humans still unknown. One very recent study reported corroborate our arguments that long-term olfactory dysfunction occurred in patients with ZIKV-associated GBS, while more ZIKV infected individuals of different age still need to be enrolled in the following studies.

Taken together, our findings characterize ZIKV infectivity and pathogenesis in olfactory system using both *in vitro* and *in vivo* models. We demonstrated the high susceptibility of olfactory tissues in both human organoids and immunodeficient mice and showed that ZIKV mainly targets OECs and several other cell types in the OM, which suggests that the olfactory pathway is a reservoir for ZIKV infection and may serve as a route of CNS invasion. Infection with ZIKV caused transient olfactory dysfunction in adult ICR mice when they were exposed to ZIKV during the neonatal period. Additionally, we noted that ZIKV induces broad-spectrum cytokine secretion in both the OM and OB and results in the dysregulation of many host genes, which may contribute to the pathogenesis of ZIKV in the olfactory

system. Further studies that aim to understand the mechanisms of viral pathogenesis in susceptible olfactory cells will benefit the development of novel target-based therapies for ZIKV.

Contributors

C.-F.Q., J.Z., M.-Y.G. and J.-F.L. conceived the project and designed the experiments. J.Z. and M.Y.G. performed the majority of the experiments and analyzed the data; R.-T.L., G.Y., L.L. and Y.-N.Q. contributed specific experiments and data analysis. C.-F.Q., J.Z., R.-T.L. wrote the manuscript with all the input from all authors. C.F.Q. supervised the study. All authors read and approved the contents of the manuscript.

Data sharing statement

The RNA-seq data reported in the present paper have been deposited to the NCBI Gene Expression Omnibus (GEO) datasets under accession number GSE214567. All software tools and platforms used here are publicly available. All of the other data that supporting the findings of this study are present in the paper and/or the Supplementary Materials. Additional data related to this paper may be requested from the authors.

Declaration of interests

The authors declare that they have no conflict of interests.

Acknowledgment

J.Z. was supported by Youth Program of National Natural Science Foundation of China (No. 82002148) from NSFC, and the China Postdoctoral Science Fund (No. 2020T130134ZX, 2020M673685). R.-T.L. was supported by the China Postdoctoral Science Fund (No. 2019M664012 and No. 2020T130135ZX). J.-F.L. was supported by the Natural Science Foundation of Beijing (7212090). C.-F.Q. was supported by the National Science Fund for Distinguished Young Scholar (No. 81925025), and the Innovative Research Group (No. 81621005) from the NSFC, and the Innovation Fund for Medical Sciences (No. 2019RU040) from the Chinese Academy of Medical Sciences (CAMS).

Appendix A. Supplementary data

Supplementary data related to this article can be found at https://doi.org/10.1016/j.ebiom.2023.104457.

References

1 Dick GW, Kitchen SF, Haddow AJ. Zika virus. I. Isolations and serological specificity. *Trans R Soc Trop Med Hyg*. 1952;46(5):509–520.
2 Petersen LR, Jamieson DJ, Powers AM, Honein MA. Zika virus. *N Engl J Med*. 2016;374(16):1552–1563.
3 Baud D, Gubler DJ, Schaub B, Lanteri MC, Musso D. An update on Zika virus infection. *Lancet*. 2017;390(10107):2099–2109.
4 Duffy MR, Chen TH, Hancock WT, et al. Zika virus outbreak on Yap Island, Federated States of Micronesia. *N Engl J Med*. 2009;360(24):2536–2543.
5 Musso D, Nilles EJ, Cao-Lormeau VM. Rapid spread of emerging Zika virus in the Pacific area. *Clin Microbiol Infect*. 2014;20(10):O595–O596.
6 Musso D, Ko AI, Baud D. Zika virus infection - after the pandemic. *N Engl J Med*. 2019;381(15):1444–1457.
7 Ruchusatsawat K, Wongjaroen P, Posanacharoen A, et al. Long-term circulation of Zika virus in Thailand: an observational study. *Lancet Infect Dis*. 2019;19(4):439–446.
8 Sasmono RT, Dhenni R, Yohan B, et al. Zika virus seropositivity in 1-4-year-old children, Indonesia, 2014. *Emerg Infect Dis*. 2018;24(9):1740–1743.
9 Musso D, Gubler DJ. Zika virus. *Clin Microbiol Rev*. 2016;29(3):487–524.
10 Simpson DI. Zika virus infection in man. *Trans R Soc Trop Med Hyg*. 1964;58:335–338.
11 Cao-Lormeau VM, Blake A, Mons S, et al. Guillain-Barré Syndrome outbreak associated with Zika virus infection in French Polynesia: a case-control study. *Lancet*. 2016;387(10027):1531–1539.
12 Carteaux G, Maquart M, Bedet A, et al. Zika virus associated with meningoencephalitis. *N Engl J Med*. 2016;374(16):1595–1596.
13 Roos RP. Zika virus-a public health emergency of international concern. *JAMA Neurol*. 2016;73(12):1395–1396.
14 Brasil P, Pereira Jr JP, Moreira ME, et al. Zika virus infection in pregnant women in Rio de Janeiro. *N Engl J Med*. 2016;375(24):2321–2334.
15 Miner JJ, Cao B, Govero J, et al. Zika virus infection during pregnancy in mice causes placental damage and fetal demise. *Cell*. 2016;165(5):1081–1091.
16 de Oliveira WK, Carmo EH, Henriques CM, et al. Zika virus infection and associated neurologic disorders in Brazil. *N Engl J Med*. 2017;376(16):1591–1593.
17 Leonhard SE, Bresani-Salvi CC, Lyra Batista JD, et al. Guillain-Barré syndrome related to Zika virus infection: a systematic review and meta-analysis of the clinical and electrophysiological phenotype. *PLoS Negl Trop Dis*. 2020;14(4):e0008264.
18 Moore CA, Staples JE, Dobyns WB, et al. Characterizing the pattern of anomalies in congenital Zika syndrome for pediatric clinicians. *JAMA Pediatr*. 2017;171(3):288–295.
19 Ireland DDC, Manangeeswaran M, Lewkowicz AP, et al. Long-term persistence of infectious Zika virus: inflammation and behavioral sequela in mice. *PLoS Pathog*. 2020;16(12):e1008689.
20 Nielsen-Saines K, Brasil P, Kerin T, et al. Delayed childhood neurodevelopment and neurosensory alterations in the second year of life in a prospective cohort of ZIKV-exposed children. *Nat Med*. 2019;25(8):1213–1217.
21 Einspieler C, Utsch F, Brasil P, et al. Association of infants exposed to prenatal Zika virus infection with their clinical, neurologic, and developmental status evaluated via the general movement assessment tool. *JAMA Netw Open*. 2019;2(1):e187235.
22 Moura da Silva AA, Ganz JS, Sousa PD, et al. Early growth and neurologic outcomes of infants with probable congenital Zika virus syndrome. *Emerg Infect Dis*. 2016;22(11):1953–1956.
23 van der Linden V, Pessoa A, Dobyns W, et al. Description of 13 infants born during October 2015-January 2016 with congenital Zika virus infection without microcephaly at birth - Brazil. *MMWR Morb Mortal Wkly Rep*. 2016;65(47):1343–1348.
24 Kapogiannis BG, Chakhtoura N, Hazra R, Spong CY. Bridging knowledge gaps to understand how Zika virus exposure and infection affect child development. *JAMA Pediatr*. 2017;171(5):478–485.
25 Satterfield-Nash A, Kotzky K, Allen J, et al. Health and development at age 19-24 months of 19 children who were born with microcephaly and laboratory evidence of congenital Zika virus infection during the 2015 Zika virus outbreak - Brazil, 2017. *MMWR Morb Mortal Wkly Rep*. 2017;66(49):1347–1351.
26 Wheeler AC. Development of infants with congenital Zika syndrome: what do we know and what can we expect? *Pediatrics*. 2018;141(Suppl 2):S154–S160.
27 Sarno M, Sacramento GA, Khouri R, et al. Zika virus infection and stillbirths: a case of hydrops fetalis, hydranencephaly and fetal demise. *PLoS Negl Trop Dis*. 2016;10(2):e0004517.
28 Calvet G, Aguiar RS, Melo ASO, et al. Detection and sequencing of Zika virus from amniotic fluid of fetuses with microcephaly in Brazil: a case study. *Lancet Infect Dis*. 2016;16(6):653–660.
29 Martines RB, Bhatnagar J, Keating MK, et al. Notes from the field: evidence of Zika virus infection in brain and placental tissues from two congenitally infected newborns and two fetal losses–Brazil, 2015. *MMWR Morb Mortal Wkly Rep*. 2016;65(6):159–160.
30 Tang H, Hammack C, Ogden SC, et al. Zika virus infects human cortical neural progenitors and attenuates their growth. *Cell Stem Cell*. 2016;18(5):587–590.
31 Cugola FR, Fernandes IR, Russo FB, et al. The Brazilian Zika virus strain causes birth defects in experimental models. *Nature*. 2016;534(7606):267–271.
32 Dang J, Tiwari SK, Lichinchi G, et al. Zika virus depletes neural progenitors in human cerebral organoids through activation of the innate immune receptor TLR3. *Cell Stem Cell*. 2016;19(2):258–265.
33 Garcez PP, Loiola EC, Madeiro da Costa R, et al. Zika virus impairs growth in human neurospheres and brain organoids. *Science*. 2016;352(6287):816–818.
34 Bell TM, Field EJ, Narang HK. Zika virus infection of the central nervous system of mice. *Arch Gesamte Virusforsch*. 1971;35(2):183–193.
35 Nowakowski TJ, Pollen AA, Di Lullo E, Sandoval-Espinosa C, Bershteyn M, Kriegstein AR. Expression analysis highlights AXL as a candidate Zika virus entry receptor in neural stem cells. *Cell Stem Cell*. 2016;18(5):591–596.

36 Bhatnagar J, Rabeneck DB, Martines RB, et al. Zika virus RNA replication and persistence in brain and placental tissue. *Emerg Infect Dis*. 2017;23(3):405–414.
37 Bayer A, Lennemann NJ, Ouyang Y, et al. Type III interferons produced by human placental trophoblasts confer protection against Zika virus infection. *Cell Host Microbe*. 2016;19(5):705–712.
38 Benjamin I, Fernández G, Figueira JV, Parpacén L, Urbina MT, Medina R. Zika virus detected in amniotic fluid and umbilical cord blood in an in vitro fertilization-conceived pregnancy in Venezuela. *Fertil Steril*. 2017;107(6):1319–1322.
39 Chen JC, Wang Z, Huang H, et al. Infection of human uterine fibroblasts by Zika virus in vitro: implications for viral transmission in women. *Int J Infect Dis*. 2016;51:139–140.
40 Govero J, Esakky P, Scheaffer SM, et al. Zika virus infection damages the testes in mice. *Nature*. 2016;540(7633):438–442.
41 Murray KO, Gorchakov R, Carlson AR, et al. Prolonged detection of Zika virus in vaginal secretions and whole blood. *Emerg Infect Dis*. 2017;23(1):99–101.
42 Barzon L, Pacenti M, Franchin E, et al. Infection dynamics in a traveller with persistent shedding of Zika virus RNA in semen for six months after returning from Haiti to Italy, January 2016. *Euro Surveill*. 2016;21(32):30316.
43 Mansuy JM, Dutertre M, Mengelle C, et al. Zika virus: high infectious viral load in semen, a new sexually transmitted pathogen? *Lancet Infect Dis*. 2016;16(4):405.
44 Ma W, Li S, Ma S, et al. Zika virus causes testis damage and leads to male infertility in mice. *Cell*. 2016;167(6):1511–1524.e10.
45 Sheng Z, Gao N, Fan D, et al. Zika virus disrupts the barrier structure and absorption/secretion functions of the epididymis in mice. *PLoS Negl Trop Dis*. 2021;15(3):e0009211.
46 Liu S, DeLalio LJ, Isakson BE, Wang TT. AXL-mediated productive infection of human endothelial cells by Zika virus. *Circ Res*. 2016;119(11):1183–1189.
47 Hamel R, Dejarnac O, Wichit S, et al. Biology of Zika virus infection in human skin cells. *J Virol*. 2015;89(17):8880–8896.
48 Miner JJ, Sene A, Richner JM, et al. Zika virus infection in mice causes panuveitis with shedding of virus in tears. *Cell Rep*. 2016;16(12):3208–3218.
49 Adams Waldorf KM, Stencel-Baerenwald JE, Kapur RP, et al. Fetal brain lesions after subcutaneous inoculation of Zika virus in a pregnant nonhuman primate. *Nat Med*. 2016;22(11):1256–1259.
50 Vielle NJ, García-Nicolás O, Oliveira Esteves BI, Brügger M, Summerfield A, Alves MP. The human upper respiratory tract epithelium is susceptible to flaviviruses. *Front Microbiol*. 2019;10:811.
51 Leung GH, Baird RW, Druce J, Anstey NM. Zika virus infection in Australia following a monkey bite in Indonesia. *Southeast Asian J Trop Med Public Health*. 2015;46(3):460–464.
52 Swaminathan S, Schlaberg R, Lewis J, Hanson KE, Couturier MR. Fatal Zika virus infection with secondary nonsexual transmission. *N Engl J Med*. 2016;375(19):1907–1909.
53 van Riel D, Verdijk R, Kuiken T. The olfactory nerve: a shortcut for influenza and other viral diseases into the central nervous system. *J Pathol*. 2015;235(2):277–287.
54 Plakhov IV, Arlund EE, Aoki C, Reiss CS. The earliest events in vesicular stomatitis virus infection of the murine olfactory neuroepithelium and entry of the central nervous system. *Virology*. 1995;209(1):257–262.
55 Becker Y. HSV-1 brain infection by the olfactory nerve route and virus latency and reactivation may cause learning and behavioral deficiencies and violence in children and adults: a point of view. *Virus Gene*. 1995;10(3):217–226.
56 Park CH, Ishinaka M, Takada A, et al. The invasion routes of neurovirulent A/Hong Kong/483/97 (H5N1) influenza virus into the central nervous system after respiratory infection in mice. *Arch Virol*. 2002;147(7):1425–1436.
57 Monath TP, Cropp CB, Harrison AK. Mode of entry of a neurotropic arbovirus into the central nervous system. Reinvestigation of an old controversy. *Lab Invest*. 1983;48(4):399–410.
58 Yamada M, Nakamura K, Yoshii M, Kaku Y, Narita M. Brain lesions induced by experimental intranasal infection of Japanese encephalitis virus in piglets. *J Comp Pathol*. 2009;141(2–3):156–162.
59 Ozdener MH, Donadoni M, Cicalese S, et al. Zika virus infection in chemosensory cells. *J Neurovirol*. 2020;26(3):371–381.
60 Lazarini F, Lannuzel A, Cabié A, et al. Olfactory outcomes in Zika virus-associated Guillain-Barré syndrome. *Eur J Neurol*. 2022;29(9):2823–2831.
61 Deng YQ, Zhang NN, Li XF, et al. Intranasal infection and contact transmission of Zika virus in Guinea pigs. *Nat Commun*. 2017;8(1):1648.
62 van der Linden V, Filho EL, Lins OG, et al. Congenital Zika syndrome with arthrogryposis: retrospective case series study. *BMJ*. 2016;354:i3899.
63 Ye Q, Zhou J, He Q, et al. SARS-CoV-2 infection in the mouse olfactory system. *Cell Discov*. 2021;7(1):49.
64 Håglin S, Bohm S, Berghard A. Single or repeated ablation of mouse olfactory epithelium by methimazole. *Bio Protoc*. 2021;11(8):e3983.
65 Qiu HY, Zhang NN, Ma QQ, et al. Aerosolized Zika virus infection in Guinea pigs. *Emerg Microb Infect*. 2022;11(1):2350–2358.
66 Li S, Armstrong N, Zhao H, et al. Zika virus fatally infects wild type neonatal mice and replicates in central nervous system. *Viruses*. 2018;10(1):49.
67 Yu L, Wang R, Gao F, et al. Delineating antibody recognition against Zika virus during natural infection. *JCI Insight*. 2017;2(12):e93042.
68 Rossi SL, Tesh RB, Azar SR, et al. Characterization of a novel murine model to study Zika virus. *Am J Trop Med Hyg*. 2016;94(6):1362–1369.
69 Charan J, Kantharia ND. How to calculate sample size in animal studies? *J Pharmacol Pharmacother*. 2013;4(4):303–306.
70 Melo AS, Aguiar RS, Amorim MM, et al. Congenital Zika virus infection: beyond neonatal microcephaly. *JAMA Neurol*. 2016;73(12):1407–1416.
71 Rasmussen SA, Jamieson DJ, Honein MA, Petersen LR. Zika virus and birth defects–reviewing the evidence for causality. *N Engl J Med*. 2016;374(20):1981–1987.
72 Miranda 2nd HA, Costa MC, Frazão MAM, Simão N, Franchischini S, Moshfeghi DM. Expanded spectrum of congenital ocular findings in microcephaly with presumed Zika infection. *Ophthalmology*. 2016;123(8):1788–1794.
73 Cui L, Zou P, Chen E, et al. Visual and motor deficits in grown-up mice with congenital Zika virus infection. *EBioMedicine*. 2017;20:193–201.
74 Yockey LJ, Varela L, Rakib T, et al. Vaginal exposure to Zika virus during pregnancy leads to fetal brain infection. *Cell*. 2016;166(5):1247–1256.e4.
75 Tian J, Pinto JM, Cui X, et al. Sendai virus induces persistent olfactory dysfunction in a murine model of PVOD via effects on apoptosis, cell proliferation, and response to odorants. *PLoS One*. 2016;11(7):e0159033.
76 Meinhardt J, Radke J, Dittmayer C, et al. Olfactory transmucosal SARS-CoV-2 invasion as a port of central nervous system entry in individuals with COVID-19. *Nat Neurosci*. 2021;24(2):168–175.
77 McMinn PC, Dalgarno L, Weir RC. A comparison of the spread of Murray Valley encephalitis viruses of high or low neuroinvasiveness in the tissues of Swiss mice after peripheral inoculation. *Virology*. 1996;220(2):414–423.
78 Mutso M, St John JA, Ling ZL, et al. Basic insights into Zika virus infection of neuroglial and brain endothelial cells. *J Gen Virol*. 2020;101(6):622–634.
79 Dando SJ, Mackay-Sim A, Norton R, et al. Pathogens penetrating the central nervous system: infection pathways and the cellular and molecular mechanisms of invasion. *Clin Microbiol Rev*. 2014;27(4):691–726.